Available online at www.sciencedirect.com
ScienceDirect
Journal of Catalysis 244 (2006) 169–182
JOURNAL OF CATALYSIS
www.elsevier.com/locate/jcat

A combined transient in situ FTIR and flow reactor study of NO_X storage and reduction over $M/BaCO_3/Al_2O_3$ (M = Pt, Pd or Rh) catalysts

Hussam Abdulhamid [a,b,*], Jazaer Dawody [a,c], Erik Fridell [a,c,1], Magnus Skoglundh [a,b]

[a] *Competence Centre for Catalysis, Chalmers University of Technology, SE-412 96 Göteborg, Sweden*
[b] *Department of Chemical and Biological Engineering – Applied Surface Chemistry, Chalmers University of Technology, SE 412 96 Göteborg, Sweden*
[c] *Department of Applied Physics, Chalmers University of Technology, SE-412 96 Göteborg, Sweden*

Received 5 May 2006; revised 27 August 2006; accepted 1 September 2006

Available online 9 October 2006

Abstract

Transient in situ DRIFTS and flow-reactor experiments were performed to study the storage and reduction of NO_X over $Pt/BaCO_3/Al_2O_3$, $Pd/BaCO_3/Al_2O_3$, and $Rh/BaCO_3/Al_2O_3$ samples using CO, H_2, C_3H_6, or C_3H_8 as the reducing agent. The DRIFTS results show that exposure of the examined samples to NO_2 results in the formation of nitrite/nitrate peaks over alumina and barium and that the reduction of stored NO_X is influenced by the type of precious metal and reducing agent. Using CO as the reductant results in a lower NO_X reduction capacity for $Pt/BaCO_3/Al_2O_3$ compared with Pd- and Rh-based samples, whereas H_2 shows a significant ability to reduce the stored NO_X on all samples examined. In addition, the reduction with CO and C_3H_6 proceeds via the formation of isocyanate species over both barium and alumina sites. The intensity of barium-isocyanate species for $Pt/BaCO_3/Al_2O_3$ is significantly lower than the corresponding intensity for the Pd- and Rh-based samples, suggesting that the interaction between barium and Pt is lower than the corresponding interaction in the $Pd/BaCO_3/Al_2O_3$ and $Rh/BaCO_3/Al_2O_3$ samples.

Keywords: DRIFT; NO_X reduction; NO_X storage; Pt; Pd; Rh; Reducing agent; H_2; CO; C_3H_6; C_3H_8

1. Introduction

NO_X storage and reduction technology offers the possibility of reducing emissions of NO_X from vehicles operating under lean-burn conditions. The concept is based on incorporating a storage material (commonly Ba) in the conventional three-way catalyst to store NO_X ($NO + NO_2$) under lean conditions until it is saturated with NO_X. Subsequently the stored NO_X is released and reduced to N_2 by turning the engine to rich operating conditions under a short period [1].

Since the concept was introduced by Toyota in the beginning of the 1990s [2], a substantial number of studies have been performed to understand the mechanisms that control the operation of the NO_X storage catalysts using gas-phase and surface characterisation techniques. Spectroscopic techniques, including in situ Fourier transform infrared spectroscopy (FTIR), have been used to follow the evolution of different surface species under different reaction conditions [3].

Many FTIR studies are devoted to understanding the NO_X storage and reduction processes [4–15]. Some of these studies have indicated that NO_X storage occurs via the formation of nitrites and nitrates over the storage component and the support. Using a $Pt/BaCO_3/Al_2O_3$ catalyst, Fanson et al. [9] observed that nitrites are transformed to nitrates when the NO pressure is increased. Vibrational bands between 2000 and 2200 cm^{-1} were formed when propene was used to reduce the stored NO_X. These bands were correlated to isocyanato on platinum and to cyano, isocyano, and cyanato on barium [9]. For barium-based catalysts, the decrease in peak intensity for stored NO_X species (in the region 1200–1650 cm^{-1}) under regeneration with carbon-containing reductants is hard to distinguish due to overlap with barium carbonate peaks [9,16,17]. In contrast, regeneration with H_2, where no carbonate species are formed

* Corresponding author. Fax: +46 31 160062.
E-mail address: husam@chem.chalmers.se (H. Abdulhamid).
[1] Present address: IVL Swedish Environmental Research Institute, P.O. Box 5302, SE-411 33 Göteborg, Sweden.

0021-9517/$ – see front matter
doi:10.1016/j.jcat.2006.09.003

during the reduction, clearly shows the decreased intensity of the surface nitrate peaks.

The stability of stored NO_X under lean and stoichiometric (propene–air) mixtures using Pt and Pt-free barium-based catalysts was investigated by Anderson et al. [8] using combined in situ FTIR and TPD techniques. These authors showed that under lean conditions, the stability of stored NO_X was influenced mainly by the oxygen concentration, whereas under rich conditions, the partial pressure of the reductant had only a minor influence on the stability of the stored NO_X. Moreover, they pointed out the impact of NO_X spillover to Pt sites in hindering the activation of propene and thereby the NO_X reduction process.

Sedlmair et al. [4] investigated the formation of different surface species and their thermal stability during the NO_X storage period using either NO, NO_2, or NO in combination with O_2 over commercial NO_X storage catalysts. Based on the FTIR observations, they derived a reaction mechanism for NO_X adsorption. It was shown that for NO exposure, the dominant surface species were nitrites formed over barium and alumina with bands at 1537, 1440, 1422, 1380, 1340, and 1206 cm^{-1}, whereas both NO_2 and NO + O_2 exposures resulted in the formation of surface nitrate species over both barium and alumina, represented by vibrational bands at 1429, 1332, 1564 cm^{-1}, respectively. These authors also showed that the barium and aluminum nitrates were more thermally stable than the corresponding nitrite species.

In a previous study [18], we investigated the effect of the type of precious metal and reducing agent on the reduction step using flow-reactor and NO_2-TPD experiments. In the present study, we aimed to obtain a deeper understanding of the influence of these parameters on the NO_X storage and regeneration processes. Thus, we combined transient in situ FTIR investigations with flow reactor experiments to study the NO_X storage and regeneration processes using $Pt/BaCO_3/Al_2O_3$, $Pd/BaCO_3/Al_2O_3$, and $Rh/BaCO_3/Al_2O_3$ catalysts. To achieve a better understanding of the regeneration of the tested catalysts, we examined a set of reducing agents (H_2, CO, C_3H_6, and C_3H_8) and temperatures (350, 250, and 150 °C). Moreover, for more realistic comparison, we performed new flow-reactor experiments using the same catalyst materials and gas compositions during lean and rich cycling for FTIR and flow reactor experiments.

2. Experimental

2.1. Sample preparation

2.1.1. Powder samples for FTIR experiments

Three powder NO_X storage catalyst samples ($M/BaCO_3/Al_2O_3$, where M = Pt, Pd, or Rh) were prepared by wet impregnation. A $BaCO_3/Al_2O_3$ sample with a barium loading (20 wt%) was prepared by adding an aqueous solution of $Ba(NO_3)_2$ to γ-Al_2O_3 (SASOL) dispersed in milli-Q water under continuous stirring and adjusting the pH of the solution to 11 by adding NH_4OH. The sample was then freezed, freeze-dried, and calcined in air at 600 °C for 1 h. Afterward, an aqueous solution of ammonium carbamate was added under continuous stirring to the barium–alumina sample to form $BaCO_3/Al_2O_3$. Then once again, the sample was freezed, freeze-dried, and calcined in air at 500 °C for 1 h.

Nitrate solutions of Pt, Pd, or Rh were used to prepare the $Pt/BaCO_3/Al_2O_3$, $Pd/BaCO_3/Al_2O_3$, and $Rh/BaCO_3/Al_2O_3$ samples. Each precious metal precursor solution was provided to a portion of the $BaCO_3/Al_2O_3$ powder under continuous stirring for 1 h, followed by freeze-drying and calcination in air at 550 °C for 2 h, resulting in a loading of 2 wt% Pt or an equal molar amount of Pd and Rh (see Table 1).

2.1.2. Monolith samples for flow-reactor experiments

Monolith samples used in the transient reactor experiments were prepared by depositing a constant amount (250 mg) of each NO_X storage powder catalyst prepared as described in Section 2.1.1 on a monolith substrate. The substrates were immersed in a slurry, prepared by 20 wt% colloidal silica (Nyacol 2034DI, Akzo Nobel) and the powder catalyst dispersed in distilled water, until the channels were filled. The samples were then placed in an oven at 95 °C for 2 h. The procedure was repeated until the desired amount of washcoat was deposited on the monolith substrates. Finally, the samples were calcined in air at 550 °C for 1 h.

2.2. Catalyst characterisation

The BET surface area for the different catalysts was determined using a Micrometrics TriStar 3000 instrument. The precious metal dispersions were determined using N_2O dissociation. The catalysts were oxidized in 1% O_2 in Ar for 10 min at 500 °C, flushed with Ar for 5 min, reduced in 2% H_2 in Ar also for 10 min at the same temperature, and finally flushed with Ar for 10 min. After the pretreatment, the temperature was decreased to 90 °C, and the catalysts were exposed to 500 ppm N_2O in Ar, with a total flow rate of 190 ml/min, for 30 min. For platinum samples, one oxygen atom was left on one surface Pt site, whereas one N_2 molecule desorbed to the gas phase for each dissociated N_2O molecule [19]. For the Pd sample, the stoichiometric factor for oxygen chemisorption was approximated to 1, whereas for Rh, the corresponding factor was estimated to be twice as high as that for Pt or Pd [20].

Precious metal dispersion was calculated by integrating the N_2 signal ($m/e = 28$) during the dissociation period, after subtracting the amount of N_2 generated from N_2O cracking in the mass spectrometer. For Pt sample, the amount of generated N_2 molecules is assumed to be equal to the number of active platinum atoms on the catalyst surface [21]. The results are tabulated in Table 1.

2.3. Transient DRIFTS and flow reactor experiments

The in situ DRIFTS experiments were performed using a BioRad FTS6000 FTIR spectrometer equipped with DRIFTS optics and a heated reaction chamber (Harrick Scientific Praying Mantis with a DRIFTS cell), using a resolution of 2 cm^{-1}. All powder catalysts were initially stabilized in a gas mixture

Table 1
Compositions, BET surface area, and estimated noble metal dispersion for the samples

Powder samples	Pt[a] (wt%)	Pd[a] (wt%)	Rh[a] (wt%)	$BaCO_3$ (wt%)	Al_2O_3 (wt%)	BET (m^2/g)	Metal dispersion[b] (%)
$Pt/BaCO_3/Al_2O_3$	2.0	–	–	20	78.0	161	5
$Pd/BaCO_3/Al_2O_3$	–	1.09	–	20	76.9	149	12
$Rh/BaCO_3/Al_2O_3$	–	–	1.06	20	76.9	153	31

[a] Constant noble metal loading of 205 μmol.
[b] The noble metal dispersion was determined for powder samples on monolith substrates with a stoichiometry factor of 1 for Pt and Pd [19]; and 2 for Rh [20].

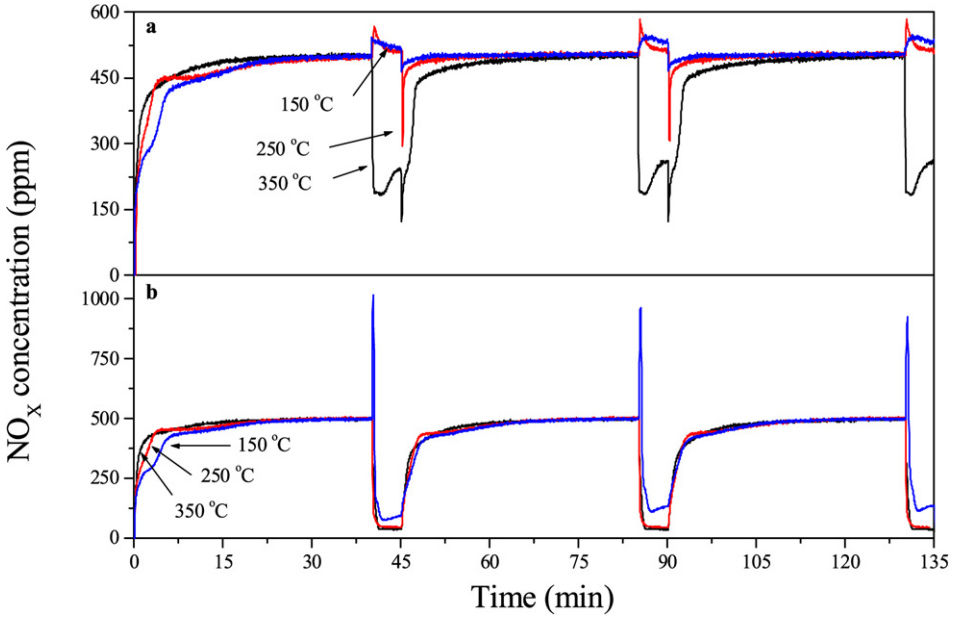

Fig. 1. NO_X storage and reduction cycles for $Pt/BaCO_3/Al_2O_3$ using (a) CO and (b) H_2 as the reducing agent at 350, 250 and 150 °C.

(with a total flow rate of 200 ml/min) consisting of 500 ppm NO_2, 800 ppm C_3H_6, and 8% O_2 balanced in Ar at 500 °C for 20 min. The catalysts were then flushed with Ar until the pretreatment temperature (400 °C) was reached. Thereafter, the catalysts were reduced with 3% H_2 for 10 min, followed by flushing in Ar for 5 min and oxidation with 8% O_2 for 10 min. Finally, the samples were cooled to the experiment temperature and left for 5 min to reach a stable catalyst temperature at which the background spectrum was collected.

Transient DRIFTS experiments were conducted at 350, 250, and 150 °C, using a constant total flow rate of 200 ml/min giving a space velocity of 106,000 h^{-1}. The pretreated catalyst was first saturated with NO_X by exposing it to 500 ppm NO_2 in Ar for 19 min. The stored NO_X was subsequently reduced by introducing a reducing agent to the NO_2/Ar flow. Thus, the regeneration gas mixture consisted of 500 ppm NO_2 and 4000 ppm CO, 4000 ppm H_2, 444 ppm C_3H_6, or 400 ppm C_3H_8 (same molar reduction capacity) balanced with Ar for 6 min. Two consecutive storage–reduction (lean–rich) cycles were conducted to follow the evolution of the surface species under the second cycle. The spectra were collected during the entire NO_X storage–reduction cycles with a time resolution of 0.5 s. A fresh sample was used for each experiment.

To correlate the evolution of surface species to the formation of gas-phase species measured under the corresponding reaction conditions, transient flow reactor experiments were performed using the same conditions as for the DRIFTS cell measurements (gas compositions, concentrations, and lean/rich cycles with 40/5 min intervals). However, the tubular reactor system has been described elsewhere [18]. The total flow rate was 2500 ml/min, corresponding to a space velocity of 75,000 h^{-1}. Finally, when comparing the flow reactor measurements with the corresponding DRIFTS measurements, it is important to take into consideration the effect of the differences in space velocity (of about 30%), mass, and heat transport in the two systems.

3. Results and discussion

3.1. NO_X storage and reduction over $Pt/BaCO_3/Al_2O_3$

To obtain an integrated understanding of the formation and disappearance of surface species during the storage and reduction periods, it is important to compare the observations from the DRIFTS study with the corresponding gas-phase measurements. Fig. 1 shows flow reactor outlet NO_X concentration for $Pt/BaCO_3/Al_2O_3$ during three consecutive lean/rich cycles at 350, 250, and 150 °C using CO and H_2 as reducing agents, respectively. Fig. 1a shows that the reduction efficiency of the $Pt/BaCO_3/Al_2O_3$ catalyst decreases with decreasing temperature when CO is used as the reducing agent. At 350 °C, the initial reduction capacity is relatively high. However, over time,

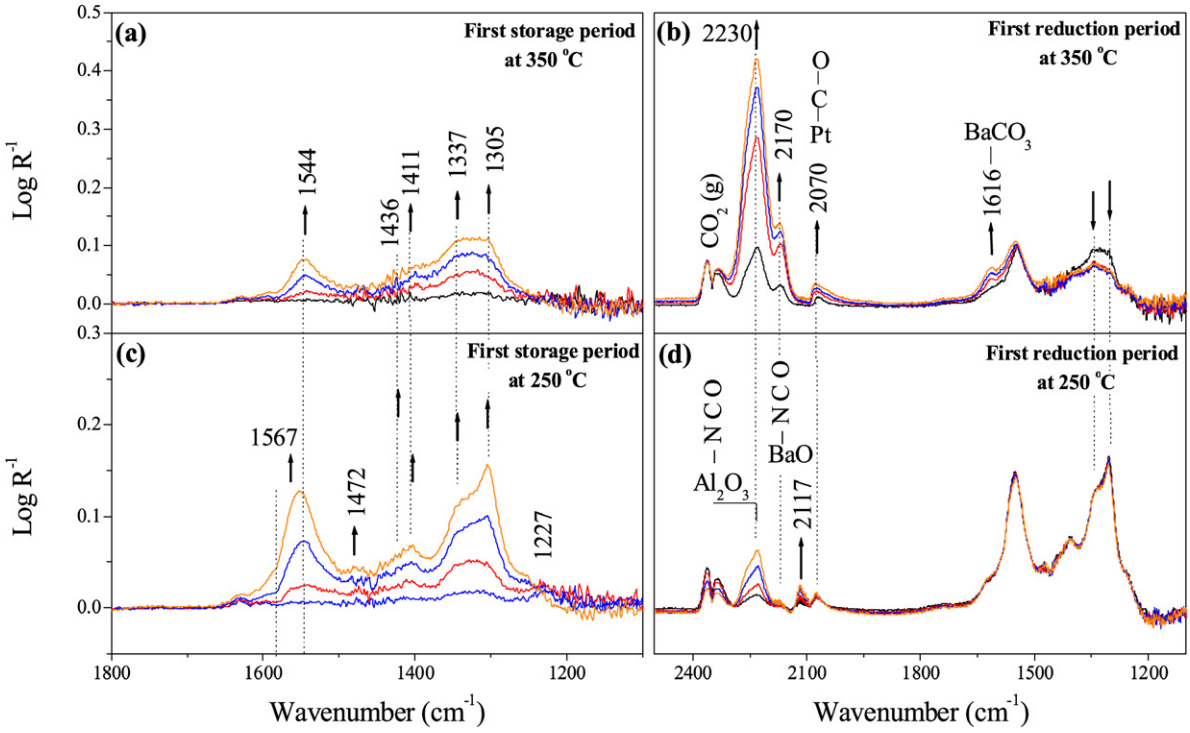

Fig. 2. DRIFT spectra for $Pt/BaCO_3/Al_2O_3$ during the first storage period (recorded after 2, 6, 12 and 18 min) and the subsequent reduction period (recorded after 2, 3, 5 and 6 min) using CO as the reducing agent at 350 (a) and (b), and 250 °C (c) and (d), respectively.

the outlet NO_X concentration increases, indicating deactivation of the reduction efficiency of the catalyst. During the active reduction period, a minor amount of N_2O is detected (not shown in Fig. 1a). At 250 and 150 °C, almost no NO_X is reduced during the rich period with CO as the reducing agent. However, a short and fast NO_X reduction is observed when switching from rich to lean conditions. A probable explanation for this is that during the reduction period, due to strong CO poisoning of the Pt sites, these sites are covered with either adsorbed CO or other C-containing species like isocyanate. When switching to the subsequent lean conditions, these species are readily oxidised by NO_2, resulting in the observed short and fast NO_X reduction.

In contrast to CO, H_2 shows considerable reduction efficiency at 350, 250, and even 150 °C. At all temperatures, the reduction is concomitant with relatively high ammonia formation (not shown), whereas a minor amount of N_2O is formed only at 250 °C.

Fig. 2 shows the corresponding DRIFTS spectra recorded after 2, 6, 12, and 18 min of the NO_X storage period and after 2, 3, 5 and 6 min of the subsequent reduction period for $Pt/BaCO_3/Al_2O_3$ catalyst at 350 and 250 °C with CO as the reducing agent. For the sake of clarity and to include the whole reduction period, we chose to show the spectra starting after 2 min of reduction. However, all spectra before the first 2 min under the reduction period were been checked, and no probable intermediates were detected. The main features observed during the first NO_X storage cycle when exposing the $Pt/BaCO_3/Al_2O_3$ sample to 500 ppm NO_2 at 350 °C are the growing bands in the 1230–1600 cm^{-1} region. The band at 1544 cm^{-1} can be assigned to bidentate nitrate over alumina [5]. The doublet bands at 1337 [$\upsilon_s(NO_2)$] with 1436 cm^{-1} [$\upsilon_{as}(NO_2)$] may be attributed to monodentate nitrate over barium [4,9]. The bands at 1305 cm^{-1} [$\upsilon_s(NO_2)$] and at 1235 cm^{-1} [$\upsilon_{as}(NO_2)$] are assigned to bridge-bonded bidentate nitrite over barium [4], whereas the band at 1411 cm^{-1} [$\upsilon(N{=}O)$] may be assigned to monodentate nitrite over barium [4]. Finally, the peak at 1472 cm^{-1} can be attributed to monodentate nitrite over alumina [4,5]. From the foregoing peak assignment, it seems that the NO_X storage occurs via the formation of nitrites and nitrates of both barium and alumina, in agreement with previous observations in the literature. It is noteworthy that the peak assignments are not precise due to the overlap between the peaks for barium nitrite/nitrate and those for alumina, particularly at low-vibration frequencies. Comparing the features observed at 350 °C with those at 250 °C (Fig. 2c) shows that the peak at 1305 cm^{-1} is more pronounced at 250 °C than at 350 °C. In addition, the peak at 1544 cm^{-1} is slightly shifted toward higher-vibration frequencies (about 1560 cm^{-1}).

In an attempt to follow the evolution of surface species during NO_X storage periods using FTIR, Pazé et al. [22] exposed a $Pt/\gamma\text{-}Al_2O_3$ sample to NO_2 at different temperatures and found that the intensity of bands in the 1350–1200 cm^{-1} and 1700–1500 cm^{-1} regions were increased with decreasing temperature. The authors related the increased band intensity, with more pronounced peak growth at 1566 and 1300 cm^{-1}, to an increased NO_X uptake on $\gamma\text{-}Al_2O_3$. Interestingly, this is almost what is found in our current study (see Fig. 2c). Thus, we believe that we have a significant NO_X storage on alumina at 250 °C. However, with increasing temperature, NO_X storage on barium becomes more significant.

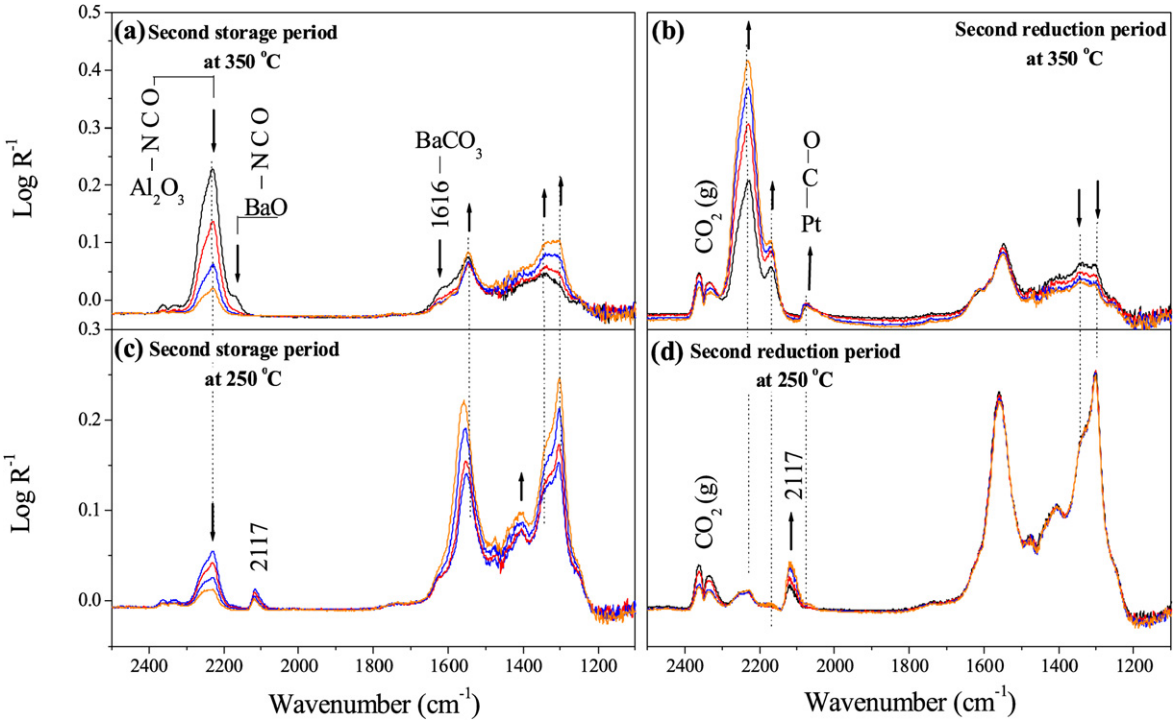

Fig. 3. DRIFT spectra for $Pt/BaCO_3/Al_2O_3$ during the second storage period (recorded after 2, 6, 12 and 18 min) and the subsequent reduction period (recorded after 2, 3, 5 and 6 min) using CO as the reducing agent at 350 (a) and (b), and 250 °C (c) and (d), respectively.

The spectra during the first NO_X reduction period at 350 °C show a decrease in the intensity of the peaks at 1337 and 1305 cm^{-1} with time, with the peak at 1616 cm^{-1} increasing simultaneously, most likely due to the formation of barium carbonate [16]. The vibrational frequencies related to barium carbonates are represented by different peaks, depending on whether surface or bulk carbonates are present [23]. These peaks consist of main and shoulder peaks [24] that can shift and/or overlap with other peaks. In addition, a significant growth of two high-intensity bands at 2230 and 2170 cm^{-1} in combination with a weak band at 2070 cm^{-1} is observed (see Fig. 2b). These peaks can most likely be assigned to surface isocyanate over alumina [25,26], either isocyanate over barium [17,27] or cyanide species over alumina [28], and linear bonded CO over platinum [29], respectively. The peak at 2170 cm^{-1} can be related to species adsorbed over barium sites, based on the investigation by Szailer et al. [17] on $Pt/BaCO_3/Al_2O_3$ and Pt/Al_2O_3 catalysts, which demonstrated a corresponding peak assigned to barium isocyanate (at around 2158 cm^{-1}) because it appeared only on the barium-containing catalyst. The decreased intensity of nitrite and nitrate species as a function of time demonstrates that at 350 °C and at the CO concentration used, the NO_X storage sites are at least partially regenerated, as is expected under oxygen deficit conditions. Because NO_2 exposure occurs under both lean and rich conditions, it is not clear whether the cyanide/isocyanate species are formed as intermediates from the reaction between the stored or gas-phase NO_X with CO. Fig. 2b shows that CO adsorption on platinum increases slightly with time (band at 2070 cm^{-1}). Correlating this observation to the continuous decrease in the reduction efficiency of the catalyst under the corresponding flow reactor experiment (Fig. 1a), we suggest that CO accumulation on the surface platinum sites is the main reason for the deteriorating reduction efficiency of the catalyst at 150 and 250 °C. At 250 °C (Fig. 2d), no decrease in the intensities of the nitrite and nitrates bands is observed, indicating that the regeneration of the NO_X storage sites is not possible using CO as a reducing agent at this temperature. In addition, the intensity of the cyanide/isocyanate peaks is significantly lower than that of the corresponding peaks observed at 350 °C. However, at 250 °C a new peak is observed at 2117 cm^{-1}. This peak increases slightly with time during the reduction period and seems to be stable, because it is observed with unchanged intensity during the subsequent second storage cycle (Fig. 3c). Accordingly, the peak at 2117 cm^{-1}, among several possibilities, could be related to CO adsorption over platinum or cyanide species adsorbed over platinum or barium sites. Bridge-bonded CO on Pt has a significantly lower vibration frequency (about 1870 cm^{-1}) [29] and is thus not likely. Mavrikakis et al. [30] have shown that the adsorption of CO on a Pt step or kink position has almost twice the binding energy than adsorption on a terrace or a side position. However, assignment of the 2117 cm^{-1} peak to CO adsorbed over Pt step or kink positions is not likely, because any CO should be easily oxidised at such a temperature under strong oxidising conditions. Taking into consideration the work of Lennartz et al. [31], who showed that cyanide adsorption on Pt(111) results in a single band between 2100 and 2130 cm^{-1}, the feature at 2117 can even be assigned to cyanide adsorbed on platinum sites. Thus, it is likely that the peak at 2117 cm^{-1} is due to accumulation of cyanide species over barium sites or in the Pt–barium interface region. This assumption is supported by the fact that the proposed cyanide species remain stable even under lean con-

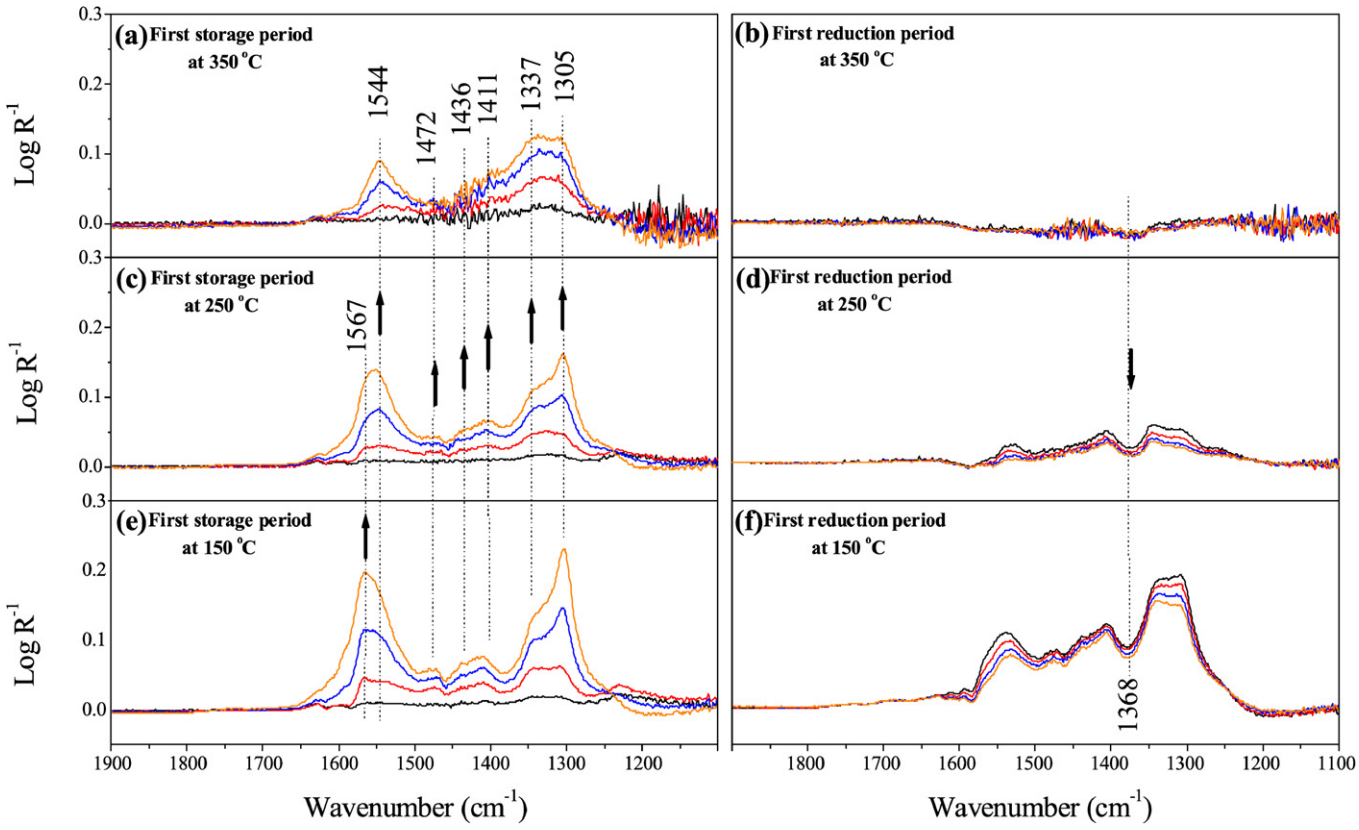

Fig. 4. DRIFT spectra for $Pt/BaCO_3/Al_2O_3$ during the first storage period (recorded after 2, 6, 12 and 18 min) and the subsequent reduction period (recorded after 2, 3, 5 and 6 min) using H_2 as the reducing agent at 350 (a) and (b), 250 (c) and (d), and 150 °C (e) and (f), respectively.

ditions and by the observed decay in the rate of reduction of stored NO_X (where spillover of NO_X from storage to Pt sites is blocked).

In addition, Fig. 3 shows that the features related to alumina and barium isocyanate formed under the first reduction period (Fig. 2) are preserved to some extent under the second NO_X storage period at both 350 and 250 °C. At both temperatures, the peaks related to nitrite and nitrate species (features in the 1600–1200 cm^{-1} region) increase only slightly, in line with the corresponding flow reactor experiment presented in Fig. 1a. It has been previously shown that the NO_X reduction process follows three main steps: (i) release of nitrite/nitrate species from the different storage sites, (ii) spillover of species between the storage sites and the precious metal sites, and (iii) a subsequent reduction by an active reducing agent over the precious metal into N_2 [32]. Therefore, the main assumed pathways to deactivate the reduction could be hindering the spillover from the storage sites to the precious metal and/or blocking the precious metal. Our DRIFTS observations during the regeneration phase with CO as the reductant suggest that at 350 °C, formation of isocyanates on both barium and alumina may hinder spillover of NO_X from these sites to platinum. Szailer et al. [17] claimed that NCO species may poison $Pt/BaCO_3/Al_2O_3$ due to the strong adsorption properties of these species, whereas CO adsorption over platinum (even with small amounts) may block these sites. In our study, the formation of the cyanide species (feature at 2117 cm^{-1}) at 250 °C may play a key role in the deterioration of the NO_X reduction process, because it is probably strongly adsorbed on the barium sites (particularly in the Pt–barium interface region), blocking these sites and preventing accessibility for the NO_X storage process.

Fig. 4 shows the different DRIFTS spectra for the first NO_X storage/reduction cycle over the $Pt/BaCO_3/Al_2O_3$ sample at 350, 250, and 150 °C using H_2 as the reductant. Figs. 4a and 2a show the same features (NO_2 exposure at 350 °C), as is also true for Figs. 4c and 2c (NO_2 exposure at 250 and 150 °C). At lower temperatures (250 and 150 °C), a new peak is observed at 1567 cm^{-1} that may be assigned to bidentate nitrite over alumina [10]. Compared with CO, the spectra during the reduction periods at 350 °C (Fig. 4b) and 250 °C (Fig. 4d) clearly reveal the high reduction efficiency of H_2.

Due to the absence of overlapping of carbonate and nitrate bands (due to the absence of any carbon source), the spectra at 350 °C show complete reduction of the adsorbed nitrite/nitrate species over the catalyst surface during the first 3 min of reduction. The appearance of a broad and slightly negative peak centered at 1368 cm^{-1} is attributed to the decomposition of a certain type of barium carbonate [16]. To clarify the appearance of this negative peak, thermodynamic calculations were performed using the commercial software HSC chemistry to study the stability of barium carbonate in the presence of hydrogen (because all samples were pretreated at higher temperature in hydrogen before the DRIFTS measurements), as well as on exposure to NO_2. The calculations show that decarbonisation of

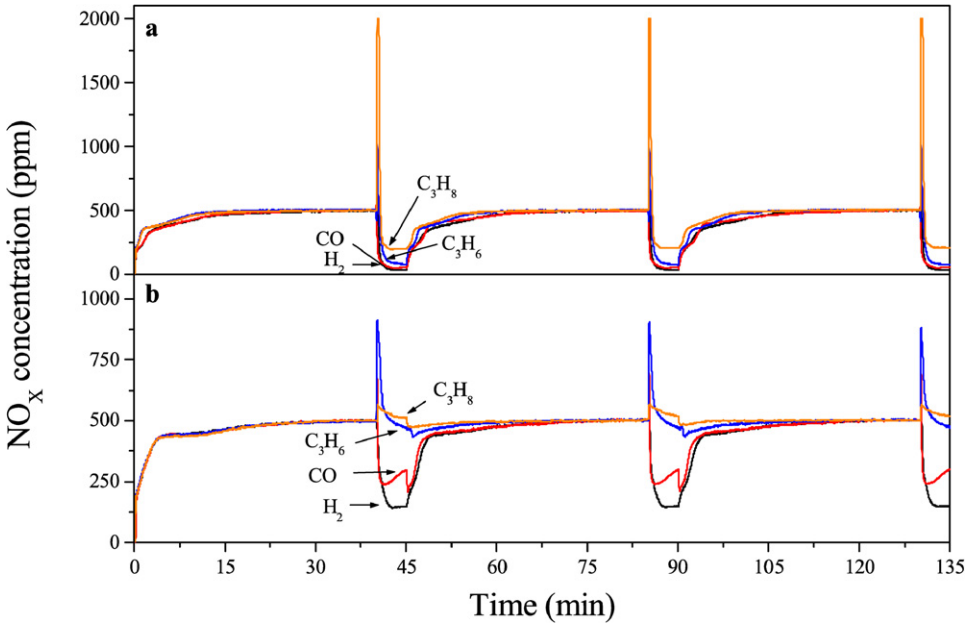

Fig. 5. NO_X storage and reduction cycles over $Pd/BaCO_3/Al_2O_3$ using either CO, H_2, C_3H_6 or C_3H_8 as the reductants at (a) 350 and (b) 250 °C.

barium carbonate is (thermodynamically) favored in the presence of H_2 at temperatures above 700 °C. In contrast, replacement of carbonate by nitrate is thermodynamically possible at room temperature. Accordingly, barium carbonate is probably stable after being pretreated with H_2, with the background collected before the NO_X storage and reduction measurements. In contrast, during the NO_X storage period with NO_2, the barium carbonate is transformed to barium nitrates via the adsorption of NO_2 and release of CO_2. This decarbonisation cannot be seen during the storage period due to the overlap with the nitrite/nitrate peaks. However, during the subsequent reduction period, where no carbon source is present in the feed, negative carbonate peaks (compared with the background spectrum of the $Pt/BaCO_3/Al_2O_3$ catalyst) appear. Because the intensity of this negative peak is rather low, we suggest that only a fraction part of barium is involved in the NSR process.

When lowering the temperature to 250 °C, a decrease in NO_X reduction efficiency is observed, with minor amounts of nitrite/nitrate species observed even at the end of the reduction period. At 150 °C, the catalytic reduction efficiency is even lower. However, the decreased intensity of the peaks at 1544 and 1305 cm^{-1} indicates that the $Pt/BaCO_3/Al_2O_3$ sample has some reduction efficiency at this temperature.

In line with the observations by Fanson et al. [9] when using H_2 as a reductant, neither ammonia nor any other intermediates could be detected on the catalyst surface (spectra range above 1800 cm^{-1} not shown in Fig. 4). This suggests that the relatively high formation of gas-phase ammonia detected during reduction proceeds rapidly.

For propene, gas-phase experiments show a relatively high reduction efficiency at 350 °C that decreases significantly when the temperature is lowered to 250 and 150 °C [33]. The corresponding DRIFTS experiments (figures not shown) show that at 350°C, the intensity of the bands at 1337 and 1305 cm^{-1} decreases only slightly during the reduction period. At the same time, a small feature appears at 2230 cm^{-1}, indicating the formation of isocyanate on alumina. At 250 °C, no decrease in the nitrite/nitrate bands is observed, indicating that propene is not able to regenerate the catalyst at this temperature. This may bring out the platinum's low ability to activate propene (under certain reducing conditions) even at 350 °C. Thus, the relatively high gas-phase reduction efficiency at 350 °C could stand for reducing the gas-phase NO_X.

Propane shows no reduction efficiency in either the gas-phase experiments or the DRIFTS study.

3.2. NO_X storage and reduction over $Pd/BaCO_3/Al_2O_3$

Fig. 5 shows the alternate gas-phase NO_X storage–reduction cycles when using CO, H_2, C_3H_6, or C_3H_8 as the reductant over the $Pd/BaCO_3/Al_2O_3$ sample at 350 and 250 °C. The figure clearly shows the high ability of $Pd/BaCO_3/Al_2O_3$ to reduce NO_X at 350 °C with any reductant used even propane, probably due its ability to activate unsaturated hydrocarbons [18].

At 250 °C, the catalyst is still able to reduce NO_X efficiently with H_2 as the reductant, whereas CO appears to impair the NO_X reduction process just after a short reduction period. However, propene and propane are almost completely unable to reduce NO_X at 250 °C.

The corresponding DRIFTS spectra for the first NO_X storage–reduction cycle over $Pd/BaCO_3/Al_2O_3$ using CO as the reductant at 350 and 250 °C are shown in Fig. 6.

In line with the corresponding gas-phase results shown in Fig. 5, the spectra recorded at 350 °C clearly show the high NO_X reduction efficiency represented by the decrease in the intensity of the different nitrite/nitrate peaks. Meanwhile, the development of peaks at 1610, 1575, and 1462 cm^{-1} during the reduction period indicates the replacement of barium nitrite/nitrate by barium carbonate [11,34]. An interesting observation during the reduction period (Fig. 6b) is the appearance

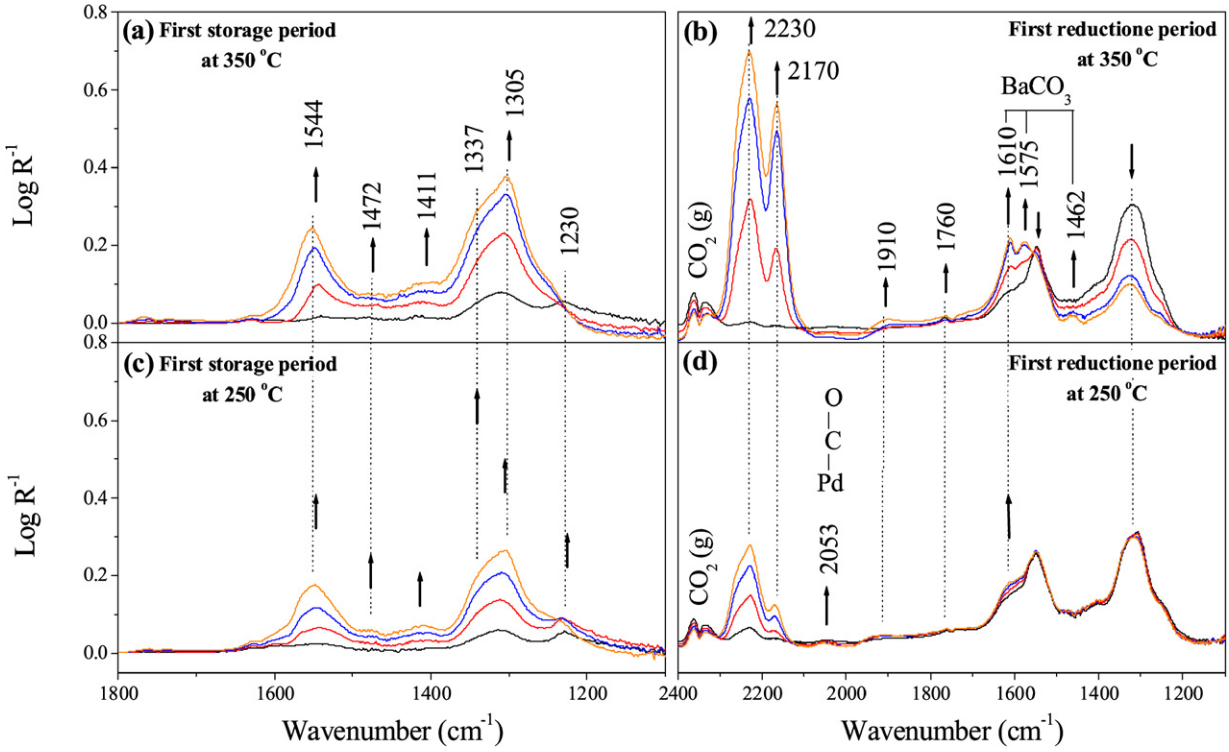

Fig. 6. DRIFT spectra for $Pd/BaCO_3/Al_2O_3$ during the first storage period (recorded after 2, 6, 12 and 18 min) and the subsequent reduction period (recorded after 2, 3, 5 and 6 min) using CO as the reducing agent at 350 (a) and (b), and 250 °C (c) and (d), respectively.

of high-intensity peaks at 2230 and 2170 cm^{-1} assigned to isocyanate over alumina and barium, respectively. The large formation of isocyanate coincident with the high NO_X reduction efficiency indicates that the formation of the isocyanate species on barium and alumina does not affect the reduction process in the case of the $Pd/BaCO_3/Al_2O_3$ sample, as was supposed to be the case for the $Pt/BaCO_3/Al_2O_3$ sample. In addition, during the reduction with CO, bands are observed in the 1950–1700 cm^{-1} range with two maxima at 1910 and 1760 cm^{-1}, which may be attributed to different configurations of NO adsorbed on palladium [35].

The NO_X storage–reduction cycle with CO at 250 °C (Figs. 6c and 6d) shows that even though some barium carbonate (band at 1610 cm^{-1}) is formed during the reduction period, the nitrite/nitrate bands are more or less stable. Analysing the spectra to interpret the deactivation of the NO_X reduction efficiency shows the evolution of a new feature at 2053 cm^{-1}. The new peak most likely can be assigned to linearly bonded CO over palladium; however, it is uncertain whether such small amount (according to its low intensity) can block the palladium sites and thus deactivate the NO_X reduction. A more reasonable explanation could be that at relatively low temperatures (250 °C), CO is not able to promote the release of the stored NO_X, and thus the availability of active Pd sites is not a key factor for the regeneration process. In contrast, the formation of isocyanate species over both alumina and barium in addition to the appearance of peaks related to adsorbed NO (resulting from NO_2 reduction) on the surface indicates that the Pd sites catalyse the reaction of CO with nitrogen-containing species resulting from the dissociation of adsorbed NO_2 over Pd.

The DRIFTS spectra for the first NO_X storage–reduction cycle when using H_2 as the reductant over $Pd/BaCO_3/Al_2O_3$ at 350 and 250 °C are shown in Fig. 7.

The spectra recorded during the reduction period at both 350 and 250 °C show significant NO_X reduction efficiency. After 2 min H_2 exposure, the nitrite/nitrate species are completely reduced; simultaneously, two main negative peaks appear at 1560 and 1320 cm^{-1}. The magnitude of these two negative peaks is significantly higher than the magnitude of the negative peak at 1368 cm^{-1} observed for the $Pt/BaCO_3/Al_2O_3$ sample under the same reaction conditions. Accordingly, we suppose that a higher fraction of barium sites in the $Pd/BaCO_3/Al_2O_3$ sample is active in the NSR process compared with the $Pt/BaCO_3/Al_2O_3$ sample. This can be due to the fact that the precious metal dispersion for the Pd-based sample is higher than that for the Pt-based sample. Also, this might be a result of a higher precious metal–barium interface area, which previously had been shown to be a key parameter in the NSR process [36]. Another interesting finding is the relationship between the barium distribution on the support surface and the NO_X storage and reduction efficiency. Our previous studies [21, 37] clearly show that the alumina surface is not entirely covered by barium in the samples prepared according to the preparation procedure used in the present study. Thus, it seems reasonable that NO_X storage occurs on both alumina and barium sites in the case of $Pt/BaCO_3/Al_2O_3$. Although no such surface characterization study was performed for $Pd/BaCO_3/Al_2O_3$, the above DRIFTS results indicate a greater precious metal–barium interaction for $Pd/BaCO_3/Al_2O_3$ than for $Pt/BaCO_3/Al_2O_3$.

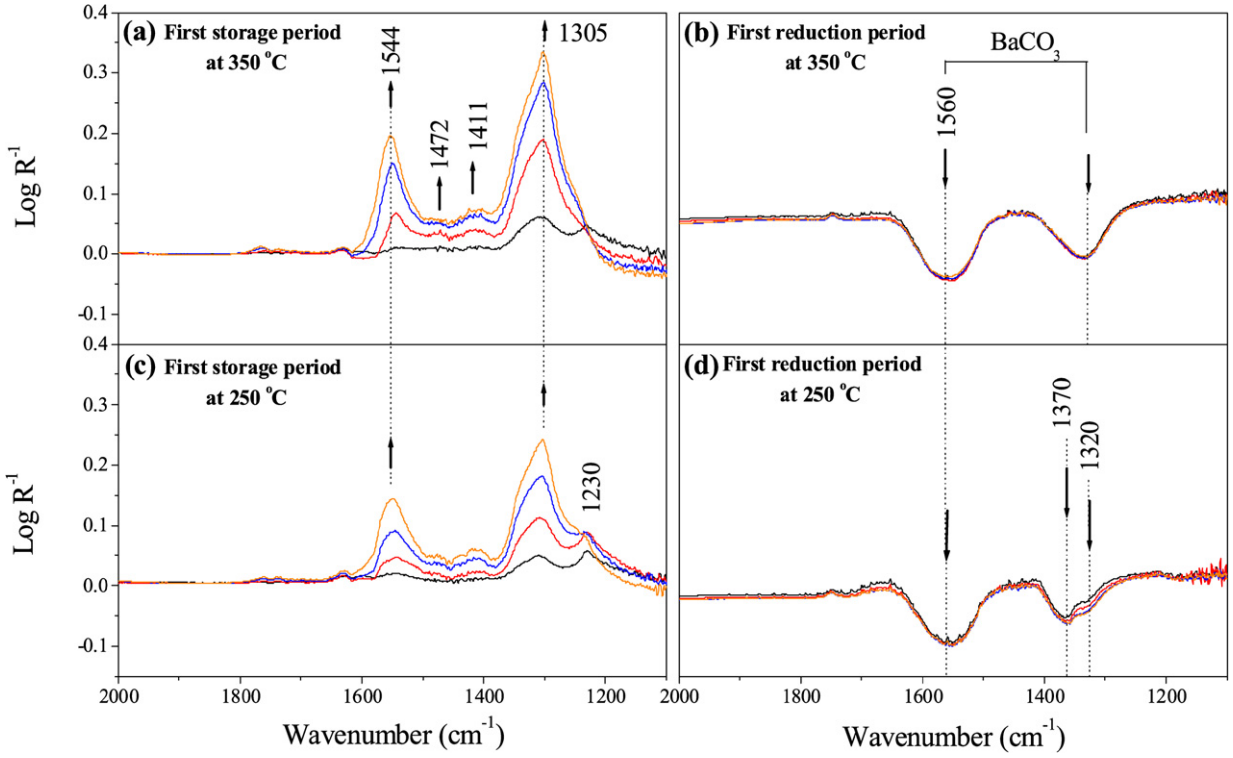

Fig. 7. DRIFT spectra for $Pd/BaCO_3/Al_2O_3$ during the first storage period (recorded after 2, 6, 12 and 18 min) and the subsequent reduction period (recorded after 2, 3, 5 and 6 min) using H_2 as the reducing agent at 350 (a) and (b), and 250 °C (c) and (d), respectively.

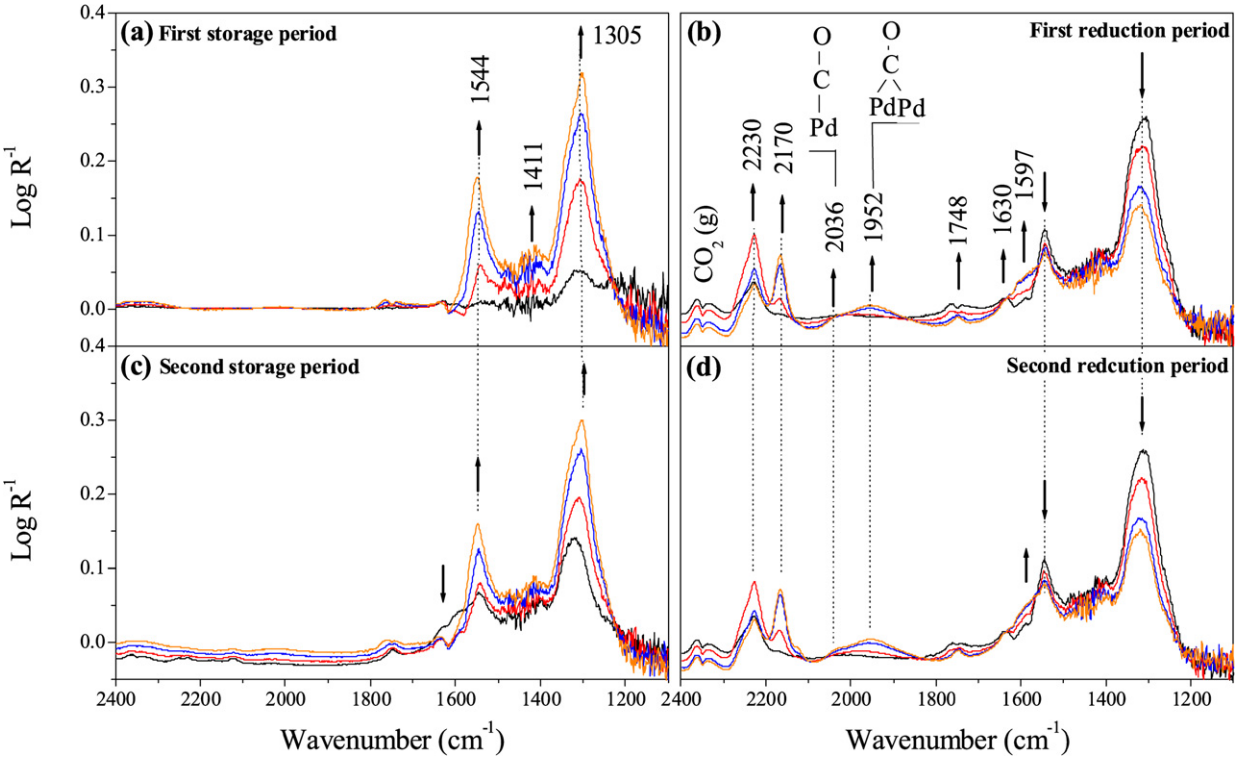

Fig. 8. DRIFT spectra for $Pd/BaCO_3/Al_2O_3$ during the first (a) and (b), and second (c) and (d), respectively, storage period (recorded after 2, 6, 12 and 18 min) and subsequent reduction period (recorded after 2, 3, 5 and 6 min) using C_3H_6 as the reducing agent at 350 °C.

Compared with the $Pt/BaCO_3/Al_2O_3$ sample, the corresponding Pd-based catalyst shows a higher regeneration capacity when using H_2 as a reductant.

For propene as the reducing agent (Fig. 8), the spectra during the reduction period show significantly decreased intensity of the bands for the barium nitrite/nitrate species, especially

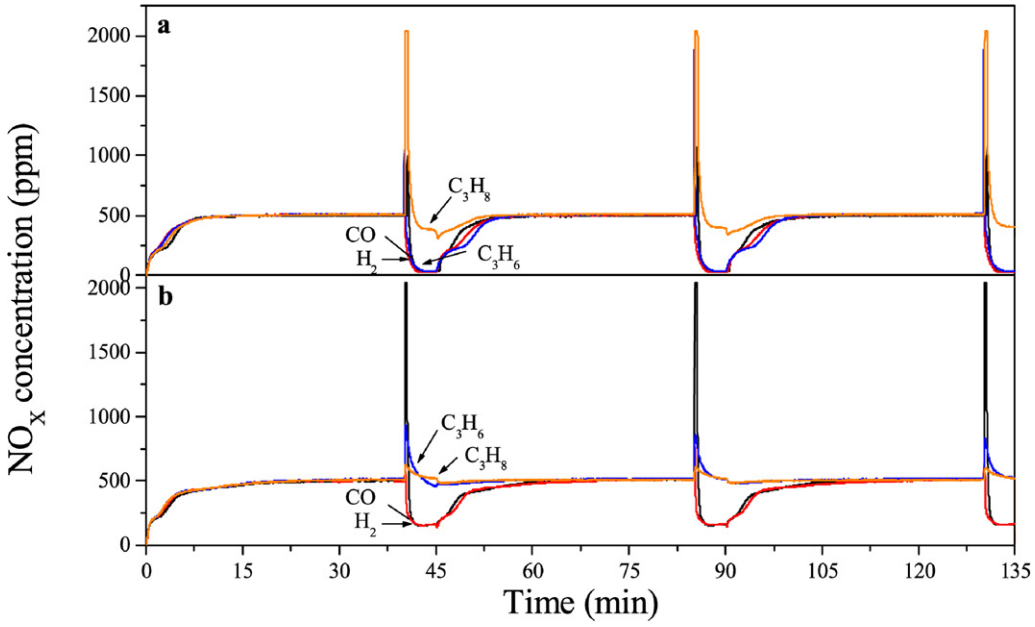

Fig. 9. NO_X storage and reduction cycles for $Rh/BaCO_3/Al_2O_3$ using either CO, H_2, C_3H_6 or C_3H_8 as the reducing agent at (a) 350 and (b) 250 °C.

for the peak at 1305 cm^{-1}. This decrease is coincident with the evolution of a barium carbonate band at 1597 cm^{-1}. In addition, the spectra for the first reduction period show the formation of isocyanate over alumina and barium (peaks at 2230 and 2170 cm^{-1}, respectively), NO adsorption on palladium (peak at 1748 cm^{-1}), and both linear and bridge-bonded CO over palladium sites (peaks at 1952 and 2036 cm^{-1}, respectively).

An interesting feature in Fig. 8 is the relatively high NO_X reduction efficiency with propene regardless of the fact that some of the palladium sites are covered with CO (Fig. 8c). The presence of CO on the palladium probably does not impair the NO_X reduction process, as was the case for the $Pt/BaCO_3/Al_2O_3$ sample. One probable interpretation could be that palladium has high activity for NO_2 dissociation, which provides sufficient oxygen on the surface to oxidise the weakly adsorbed CO.

Doi et al. [38] investigated the decomposition of N_2O over alumina-supported Pt, Pd, and Rh catalysts and found that Pd and Rh have a higher activity for N_2O decomposition compared with Pt. By analogy, Pd and Rh likely also have higher activity for NO_2 dissociation activity than Pt. Previous studies also showed that CO interacts more strongly with Pt compared with Pd as well as Rh, whereas the heat of adsorption of CO over Pt(100) is 215 kJ/mol [39], compared with 165 kJ/mol for Pd(100) [40] and 118 kJ/mol for Rh(100) [41].

However, in agreement with the gas-phase experiment (Fig. 5), the corresponding DRIFTS experiment shows that propene does not reduce the stored NO_X at 250 °C. The spectra for the reduction period at 250 °C (not shown) indicate the formation of isocyanate over alumina and CO adsorption on palladium. The low NO_X reduction activity at 250 °C is most likely due to the low temperature for activating propene over palladium (at this temperature).

3.3. NO_X storage and reduction over $Rh/BaCO_3/Al_2O_3$

Fig. 9 shows the gas-phase NO_X storage–reduction cycles over the $Rh/BaCO_3/Al_2O_3$ sample when using either CO, H_2, C_3H_6, or C_3H_8 as the reductant at 350 and 250 °C. Both CO and H_2 show high NO_X reduction efficiency at both temperatures. Using H_2 as the reductant results in the formation of ammonia (not shown in Fig. 9) at 350 and 250 °C, whereas no nitrous oxide is observed. Using H_2 as the reductant also results in a considerable NO_X breakthrough peak (1270 and 1530 ppm at 350 and 250 °C, respectively). The amounts of NO_X released in the breakthrough peak when CO is used as the reductant are 66 and 260 ppm at 350 and 250 °C, respectively. At 350 °C, C_3H_6 shows NO_X reduction efficiency comparable to that of CO and H_2, whereas at 250 °C, propene is not able to reduce the gas phase and stored NO_X. During NO_X reduction with propene, a minor amount of ammonia is detected, whereas a 1360-ppm NO_X breakthrough peak is observed when changing from lean to rich phase.

Fig. 10 shows the DRIFTS spectra for the first and second NO_X storage–reduction cycles when using CO as the reductant over the $Rh/BaCO_3/Al_2O_3$ sample at 350 °C. In agreement with gas-phase observations, the DRIFTS spectra for the first reduction period show a significant NO_X reduction efficiency with CO, as indicated by the decreased intensity of the bands for the different nitrite/nitrate species.

Formation of barium carbonate as a consequence of NO_X reduction is clearly represented by the growth of peaks at 1610 and 1578 cm^{-1}. Moreover, the spectra recorded during the reduction also show the evolution of several peaks at 2230, 2170, 2080, 2025, 1872, 1757, and 1705 cm^{-1}. The peaks at 2230 and 2170 cm^{-1} can be assigned to isocyanate species adsorbed over alumina and barium. The bands at 2080 and 2025 cm^{-1} are most likely due to CO adsorption on different Rh sites [42,43],

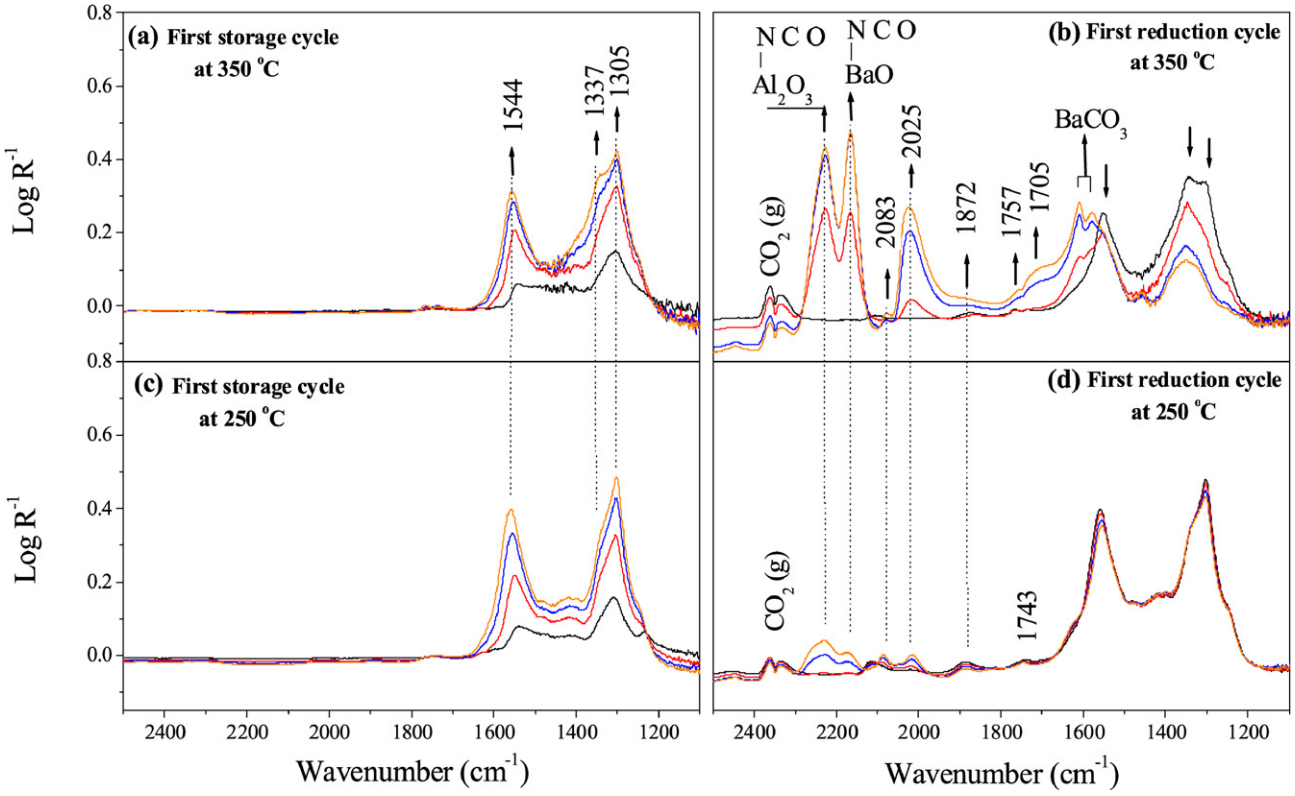

Fig. 10. DRIFT spectra for $Rh/BaCO_3/Al_2O_3$ during the first (a) and (b), and second (c) and (d), respectively, storage period (recorded after 2, 6, 12 and 18 min) and subsequent reduction period (recorded after 2, 3, 5 and 6 min) using CO as the reducing agent at 350 °C.

whereas the bands at 1872, 1775, and 1705 cm^{-1} represent different NO species adsorbed on Rh [44,45].

Similar to what occurs with Pd, CO adsorption on Rh sites (especially the band with high intensity at 2015 cm^{-1}) does not seem to hinder the NO_X reduction process at 350 °C. The high intensity of the bands attributed to NO adsorption on Rh indicates high activity of Rh to dissociate NO_2 to NO and oxygen atoms on the surface. The oxygen atoms may react with adsorbed CO. This, along with the lower adsorption characteristics of CO on Rh (compared with Pt) may explain why CO does not poison the Rh surface, maintaining efficient NO_X reduction. Moreover, the spectra during the second storage period (figure not shown) indicate fast oxidation of CO adsorbed over Rh, as well as removal of the alumina and barium-isocyanate species. Consequently, the catalyst is able to store NO_X during the second storage period. The spectra for the first NO_X storage and reduction cycle presented in Fig. 10c indicate sufficient NO_X storage capacity at 250 °C, in line with the corresponding gas-phase NO_X storage results (Fig. 9b). However, the reduction of the nitrite/nitrates in the subsequent reduction period (Fig. 10d) is significantly limited. This is in disagreement with the corresponding gas-phase results showing good NO_X storage performance during the second NO_X storage period.

Fig. 11 shows the DRIFTS spectra for the first NO_X storage–reduction cycle over the $Rh/BaCO_3/Al_2O_3$ sample using H_2 as the reductant at 350 and 250 °C. At 350 °C, the spectra show that H_2 is able to completely reduce the adsorbed nitrite/nitrate species. Similar to the case with the $Pd/BaCO_3/Al_2O_3$ catalyst, negative peaks appear at 1560 and 1320 cm^{-1} during the reduction period using H_2 as the reducing agent, due to removal of $BaCO_3$ peaks from the background. Interestingly, the magnitude of these negative peaks is rather similar for the $Pd/BaCO_3/Al_2O_3$ and the $Rh/BaCO_3/Al_2O_3$ catalysts but is significantly greater than the corresponding negative peaks observed for the $Pt/BaCO_3/Al_2O_3$ catalyst under the same condition.

At 250 °C, an obvious decrease in the intensity of the bands at 1544, 1337, and 1305 cm^{-1} is observed; however, the species are not completely removed. The spectra at both temperature show that the bands at 1544 and 1305 cm^{-1} are reduced more rapidly than the bands at 1411 and 1337 cm^{-1}. Using H_2 as the reducing agent indicates that nitrate species on alumina generally are more easily reduced than the corresponding species on barium for all of the samples investigated. Similar to the $Pt/BaCO_3/Al_2O_3$ and $Pd/BaCO_3/Al_2O_3$ samples, the spectra for the $Rh/BaCO_3/Al_2O_3$ sample show no ammonia adsorbed on the catalyst surface. Fig. 12 shows the DRIFTS spectra for the first NO_X storage–reduction cycle over the $Rh/BaCO_3/Al_2O_3$ sample when using propene as the reductant at 350 and 250 °C. The spectra reveal that at 350 °C, the propene is able to efficiently reduce the stored NO_X. During the reduction period, different peaks (between 2230 and 1700 cm^{-1}) are formed, similar to those observed during the reduction with CO (Fig. 10). This indicates that over $Rh/BaCO_3/Al_2O_3$, the reduction of NO_X may proceed via the same reaction pathway using both CO and C_3H_6 as reducing agents.

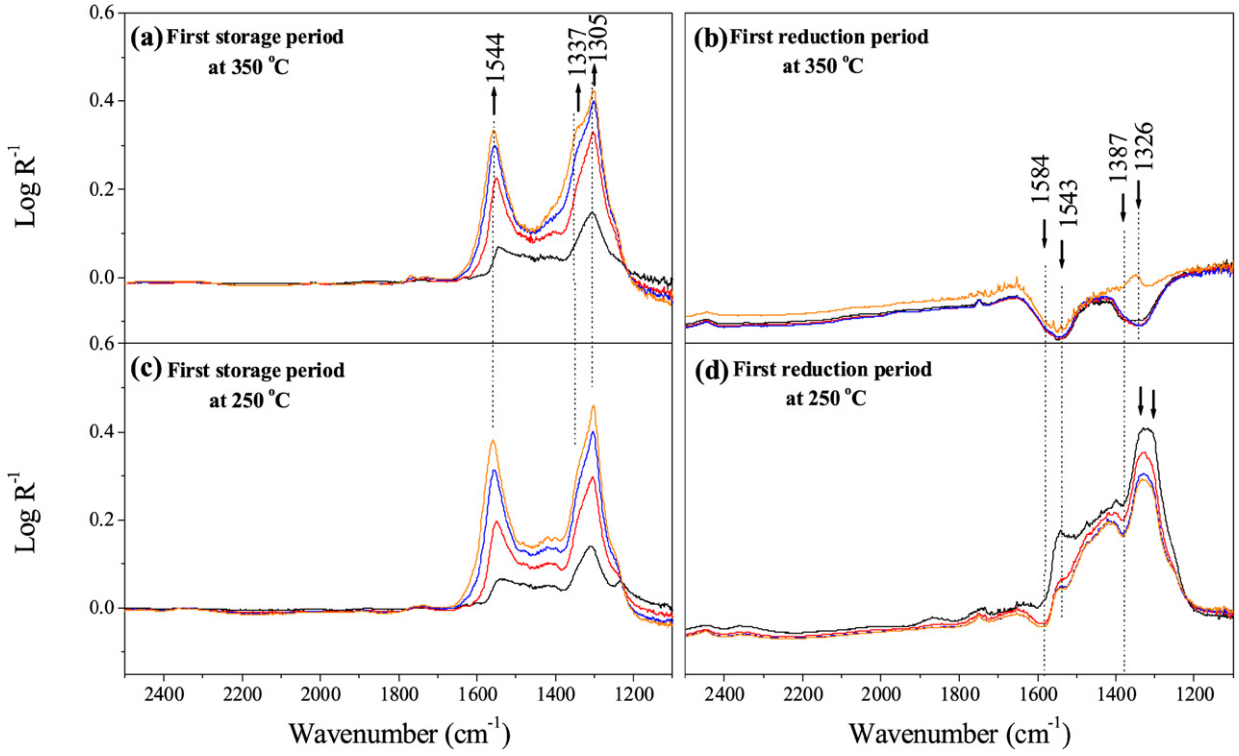

Fig. 11. DRIFT spectra for $Rh/BaCO_3/Al_2O_3$ during the first storage period (recorded after 2, 6, 12 and 18 min) and the subsequent reduction period (recorded after 2, 3, 5 and 6 min) using H_2 as the reducing agent at 350 and 250 °C.

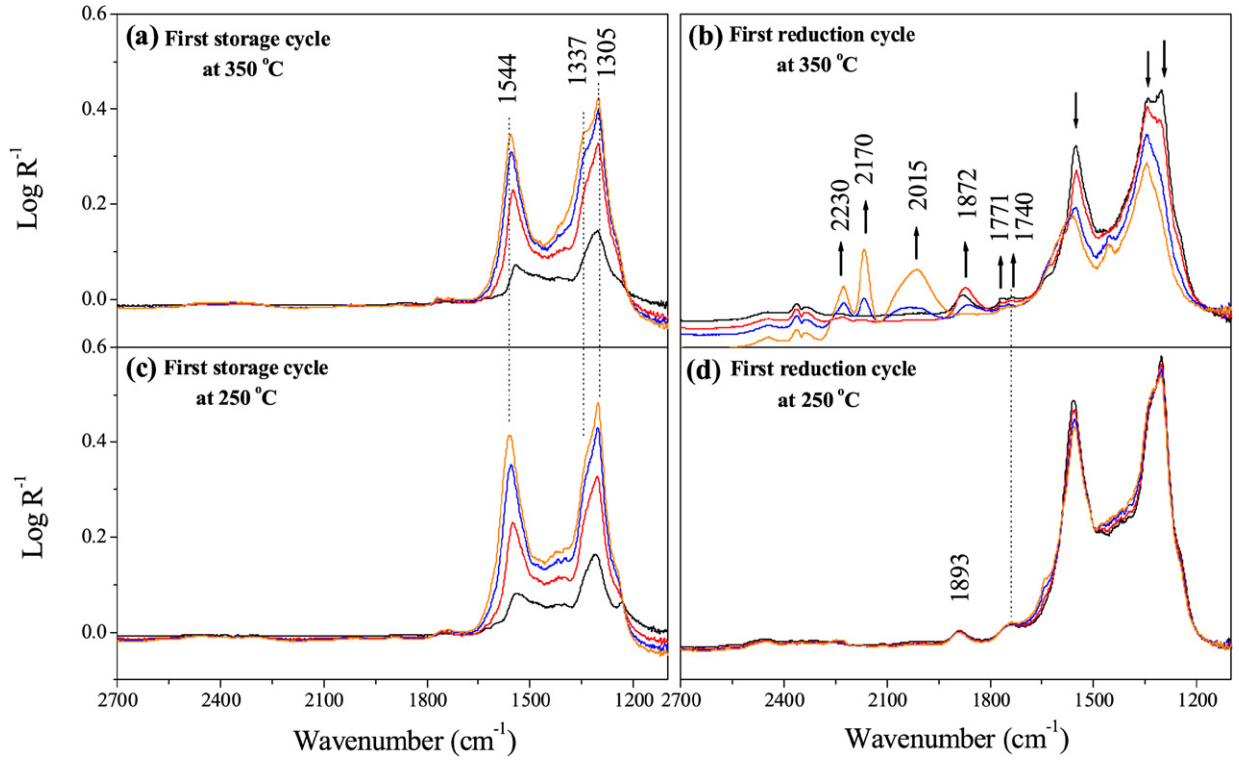

Fig. 12. DRIFT spectra for $Rh/BaCO_3/Al_2O_3$ during the first storage period (recorded after 2, 6, 12 and 18 min) and the subsequent reduction period (recorded after 2, 3, 5 and 6 min) using C_3H_6 as the reducing agent at 350 (a) and (b), and 250 °C (c) and (d), respectively.

However, at 250 °C (Fig. 12d), the spectra during the reduction period reveal the inability of propene to reduce the adsorbed NO_X; only a very small decrease in the 1544 cm^{-1} peak is seen. Further, there is no evidence of the formation of any isocyanate or CO adsorption on the surface, most likely due to low activation of propene at this temperature.

The main conclusions from our previous study [18] were that H_2 and CO had higher NO_X reduction efficiency than C_3H_6 and C_3H_8. In addition, the type of precious metal was found to affect the NO_X storage–reduction properties. The $Pd/BaCO_3/Al_2O_3$ catalyst had both high storage ability and reduction efficiency, whereas the $Rh/BaCO_3/Al_2O_3$ catalyst had high reduction efficiency but relatively low NO_X storage ability. There is a good agreement between the results of our previous study and the present study.

An interesting observation for the different precious metal catalysts is the formation of isocyanate species over barium when using a carbon-containing reducing agent. Compared with $Pt/BaCO_3/Al_2O_3$, both $Pd/BaCO_3/Al_2O_3$ and $Rh/BaCO_3/Al_2O_3$ catalysts show significantly higher ratios of isocyanate species formed over barium/alumina sites (1.1 for Rh, 0.81 for Pd, and 0.32 for Pt using CO as the reductant). This comparison indicates that the number of barium sites involved in the NO_X storage and reduction process is significantly lower in the $Pt/BaCO_3/Al_2O_3$ sample than in the $Pd/BaCO_3/Al_2O_3$ and $Rh/BaCO_3/Al_2O_3$ samples. The higher rate of barium carbonate transformation to barium nitrite and nitrate under lean conditions for the $Pd/BaCO_3/Al_2O_3$ and the $Rh/BaCO_3/Al_2O_3$ samples compared with the $Pt/BaCO_3/Al_2O_3$ sample supports this hypothesis. From these findings, we conclude that the Pt sites are probably supported mainly on the alumina, whereas both Pd and Rh seem to be dispersed on both barium and alumina sites.

Comparing the NO_X storage and reduction activities for the tested samples reveals that the intensities of the bands for the adsorbed NO_X species on the $Pd/BaCO_3/Al_2O_3$ and the $Rh/BaCO_3/Al_2O_3$ catalysts are significantly higher than those for the $Pt/BaCO_3/Al_2O_3$ catalyst. The corresponding gas-phase experiments show that the NO_X storage capacity is higher for the $Pd/BaCO_3/Al_2O_3$ and $Rh/BaCO_3/Al_2O_3$ samples than for $Pt/BaCO_3/Al_2O_3$. The difference in NO_X storage capacity for the tested catalysts may be related to the variation in the dispersion of the precious metal (Table 1) and/or the location of the precious metal sites in relation to the different storage sites.

4. Conclusion

Transient in situ DRIFTS experiments were performed to follow the evolution of various surface species during the NO_X storage and reduction processes over $Pt/BaCO_3/Al_2O_3$, $Pd/BaCO_3/Al_2O_3$, and $Rh/BaCO_3/Al_2O_3$ samples using CO, H_2, C_3H_6, or C_3H_8 as the reducing agent. In addition, NO_X storage and reduction cycles with the same experimental conditions were performed using a flow reactor system for comparison. The results from the DRIFTS measurements are in general agreement with the flow reactor experiments. However, some differences are observed, probably due to differences in space velocity, mass, and heat transfer.

For all catalysts and at all tested temperatures, exposure to NO_2 results in the formation of different nitrite/nitrate peaks over alumina and barium regardless of the type of catalyst. In contrast, the NO_X reduction seems to be related to the type of precious metal and the reducing agent. Using CO as the reducing agent results in a lower NO_X reduction capacity for $Pt/BaCO_3/Al_2O_3$ in comparison to the corresponding Pd and Rh based samples. A stronger interaction between CO and Pt compared with Pd and Rh likely suppresses the interaction between NO_2 and Pt. This may explain the observed deactivation in NO_X reduction capacity for the $Pt/BaCO_3/Al_2O_3$ sample. However, with H_2 as the reducing agent, all three samples show similar high NO_X reduction performance.

Regeneration with CO and C_3H_6 results in the formation of isocyanate species over barium and alumina sites, indicating that regeneration of the stored NO_X proceeds via the same reaction pathways for these two reducing agents. The intensity of the barium isocyanate peak for $Pt/BaCO_3/Al_2O_3$ is significantly lower than the corresponding peaks for the $Pd/BaCO_3/Al_2O_3$ and $Rh/BaCO_3/Al_2O_3$ samples during reduction with CO and C_3H_6. In addition, regeneration with carbon-containing reductants results in the appearance and growth of barium carbonate peaks accompanying a gradual decrease in the intensity of the nitrite/nitrate peaks. With H_2, the removal of nitrite/nitrates results in the appearance of negative peaks due to the removal of barium carbonate peaks from the background. The intensity of these negative peaks for $Pt/BaCO_3/Al_2O_3$ is significantly lower than that for $Pd/BaCO_3/Al_2O_3$ and $Rh/BaCO_3/Al_2O_3$, indicating that fewer barium sites are involved in the NSR process in the Pt-based sample than in the Pd- and the Rh-based samples. From these results, we relate the lower NO_X storage and regeneration performance for the $Pt/BaCO_3/Al_2O_3$ sample compared with the $Pd/BaCO_3/Al_2O_3$ and $Rh/BaCO_3/Al_2O_3$ samples to the lower precious metal dispersion and/or lower precious metal–barium interface area in the former sample compared with the latter samples.

Acknowledgments

The authors thank Dr. Henrik Grönbeck for valuable discussions. This work was performed at the Competence Centre for Catalysis, which is hosted by Chalmers University of Technology and financially supported by the Swedish Energy Agency and the member companies: AB Volvo, GM Powertrain Sweden AB, Scania CV AB, Volvo Car Corporation, Perstorp Specialty Chemicals AB, Haldor Topsøe A/S, and the Swedish Space Corporation.

References

[1] J. Feeley, M. Deeba, R.J. Farrauto, Stud. Surf. Sci. Catal. 116 (1998) 529.
[2] N. Takahashi, H. Shinjoh, T. Iijima, T. Suzuki, K. Yamazaki, K. Yokota, H. Suzuki, N. Miyoshi, S. Matsumoto, T. Tanizawa, T. Tanaka, S. Tateishi, K. Kasahara, Catal. Today 27 (1996) 63.
[3] B.M. Weckhuysen, In situ Spectroscopy of Catalysts, American Scientific Publishers, Stevenson Ranch, CA, 2004.
[4] C. Sedlmair, K. Seshan, A. Jentys, J.A. Lercher, J. Catal. 214 (2003) 308.
[5] Y. Su, M.D. Amiridis, Catal. Today 96 (2004) 31.
[6] F. Prinetto, G. Ghiotti, I. Nova, L. Lietti, E. Tronconi, P. Forzatti, J. Phys. Chem. B 105 (2001) 12732.
[7] F. Prinetto, G. Ghiotti, I. Nova, L. Castoldi, L. Lietti, E. Tronconidi, P. Forzatti, Phys. Chem. Chem. Phys. 5 (2003) 4428.
[8] J.A. Anderson, B. Bachiller-Baeza, M. Fernandez-Garcia, Phys. Chem. Chem. Phys. 5 (2003) 4418.

[9] P.T. Fanson, M.R. Horton, W.N. Delgass, J. Lauterbach, Appl. Catal. B 46 (2003) 393.
[10] I. Nova, L. Castoldi, L. Lietti, E. Tronconi, P. Forzatti, F. Prinetto, G. Ghiotti, J. Catal. 222 (2004) 377.
[11] Z. Liu, J.A. Anderson, J. Catal. 224 (2004) 18.
[12] P. Broqvist, H. Grönbeck, E. Fridell, J. Phys. Chem. B 108 (2004) 3523.
[13] E. Fridell, H. Persson, B. Westerberg, L. Olsson, M. Skoglundh, Catal. Lett. 66 (2000) 71.
[14] E. Fridell, M. Skoglundh, B. Westerberg, S. Johansson, G. Smedler, J. Catal. 183 (1999) 196.
[15] B. Westerberg, E. Fridell, J. Mol. Catal. A 165 (2001) 249.
[16] H. Mahzoul, L. Limousy, J.F. Brilhac, P. Gilot, J. Anal. Appl. Pyrol. 56 (2000) 179.
[17] T. Szailer, J.H. Kwak, D.H. Kim, J.C. Hanson, C.H.F. Peden, J. Szanyi, J. Catal. 239 (2006) 51.
[18] H. Abdulhamid, E. Fridell, M. Skoglundh, Appl. Catal. B 62 (2006) 319.
[19] M.H. Kim, J.R. Ebner, R.M. Friedman, M.A. Vannice, J. Catal. 204 (2001) 348.
[20] K. Kunimori, T. Uchijima, M. Yamada, H. Matsumoto, T. Hattori, Y. Murakami, Appl. Catal. 4 (1982) 67.
[21] J. Dawody, L. Eurenius, H. Abdulhamid, M. Skoglundh, E. Olsson, E. Fridell, Appl. Catal. A 296 (2005) 157.
[22] C. Pazé, G. Gubitosa, S.O. Giacone, G. Spoto, F.X. Llabrés i Xamena, A. Zecchina, Top. Catal. 30/31 (2004) 169.
[23] S.W. Lu, B.I. Lee, L.A. Mann, Mater. Lett. 43 (2000) 102.
[24] H. Mahzoul, J.F. Brilhac, P. Gilot, Appl. Catal. B 20 (1999) 47.
[25] M.L. Unland, J. Phys. Chem. 79 (1975) 610.
[26] F.C. Meunier, J.P. Breen, V. Zuzaniuk, M. Olsson, J.R.H. Ross, J. Catal. 187 (1999) 493.
[27] T. Lesage, C. Verrier, P. Bazin, J. Saussey, M. Daturi, Phys. Chem. Chem. Phys. 5 (2003) 4435.
[28] M. Huuhtanen, T. Kolli, T. Maunula, R.L. Keiski, Catal. Today 75 (2002) 379.
[29] M. Primet, J.M. Basset, M.V. Mathieu, M. Prettre, J. Catal. 29 (1973) 213.
[30] M. Mavrikakis, B. Hammer, J.K. Nørskov, Phys. Rev. Lett. 81 (1998) 2819.
[31] M. Lennartz, M. Arenz, C. Stuhlmann, K. Wandelt, Surf. Sci. 461 (2000) 98.
[32] W.S. Epling, L.E. Campbell, A. Yezerets, N.W. Currier, J.E. Parks, Catal. Rev. 46 (2004) 163.
[33] H. Abdulhamid, E. Fridell, M. Skoglundh, Top. Catal. 30/31 (2004) 161.
[34] F. Rohr, S.D. Peter, E. Lox, M. Kögel, A. Sassi, L. Juste, C. Rigaudeau, G. Belot, P. Gélin, M. Primet, Appl. Catal. B 56 (2005) 201.
[35] M. Valden, R.L. Keiski, N. Xiang, J. Pere, J. Aaltonen, M. Pessa, T. Maunula, A. Savimäki, A. Lahti, M. Härkönen, J. Catal. 161 (1996) 614.
[36] I. Nova, L. Lietti, L. Castoldi, E. Tronconi, P. Forzatti, J. Catal. 239 (2006) 244.
[37] J. Dawody, M. Skoglundh, S. Wall, E. Fridell, J. Mol. Catal. A 225 (2004) 259.
[38] K. Doi, Y.Y. Wu, R. Takeda, A. Matsunami, N. Arai, T. Tagawa, S. Goto, Appl. Catal. B 35 (2001) 43.
[39] Y.Y. Yeo, L. Vattuone, D.A. King, J. Chem. Phys. 104 (1996) 3810.
[40] Y.Y. Yeo, L. Vattuone, D.A. King, J. Chem. Phys. 106 (1997) 1990.
[41] R. Kose, W.A. Brown, D.A. King, J. Phys. Chem. B 103 (1999) 8722.
[42] G. Bamwenda, A. Ogata, A. Obuchi, H. Takahashi, K. Mizuno, React. Kinet. Catal. Lett. 56 (1995) 311.
[43] K.A. Almusaiteer, S.S.C. Chuang, J. Phys. Chem. B 104 (2000) 2265.
[44] P. Granger, H. Praliaud, J. Billy, L. Leclercq, G. Leclercq, Surf. Interface Anal. 34 (2002) 92.
[45] J. Rasko, Z. Szabo, T. Bansagi, F. Solymosi, Phys. Chem. Chem. Phys. 3 (2001) 4437.